E-proceedings of the 38th IAHR World Congress
September 1-6, 2019, Panama City, Panama
doi:10.3850/38WC092019-1739X

A SHOCK FITTING APPROACH FOR SIMULATING THE SURGE CAUSED BY OBSTRUCTION IN A STORM-WATER TUNNEL

ARMAN ROKHZADI[(1),] & MUSANDJI FUAMBA[(2)]
[(1,2)] Dept. Civil, Geological and Mining Engineering, Polytechnique Montreal, Montréal, Quebec, Canada.
email:arman.rokhzadi@polymtl.ca; musandji.fuamba@polymtl.ca

ABSTRACT

During intense rain and flood situation, the gravity flow in sewer network transients to a partially pressurized flow, in which the air pocket is entrapped and undergone intense compression. Severe surging resulting from large compressed air pocket may lead to operational failures and structural damage. A typical approach to simulate these surge flows is interrupting the downstream end by partially or completely closing a gate valve. Besides experimental efforts, the relevant numerical simulations have attracted a lot of attention due to the cost-effectiveness. Some numerical studies simplify the governing equations by adopting a lumped inertia approach (rigid column model) to simulate the unsteady flow. Meanwhile, in other studies, the modified Saint-Venant equations were used to incorporate the pipe elasticity to take into account the effects of water compressibility. Recently, the authors performed a simulation using a shock-fitting approach, in which the free-surface Saint-Venant equations in conjunction with the rigid column model are employed to simulate the air pocket entrapment in a closed-conduit transient flow. In this paper, the performance of this approach was compared to other approaches in the previous studies. It was found that this shock-fitting approach outperforms the other methods in terms of calculating the maximum and minimum peak surge heads as well as the consecutive attenuations. This improvement was observed, particularly, for completely blocking the outflow with various ranges of the air pocket sizes and discharged flowrates.

Keywords: Transient closed conduit flows; Surge pressure; Shock fitting; rigid column; Free-surface flow.

1 INTRODUCTION

A free-surface flow in a closed conduit below grade system, which transports the ground water and rainfall, may change to an under pressure flow, due to sudden changes in the boundary conditions, i.e. blockage or larger flowrates than the capacity along the sewer system. Therefore, the gravity flow transients to a pressurized flow and the air pocket, which is entrapped and undergone an intense compression, could abruptly escape either from the upstream or downstream manholes. The operational problems, damaging effects to the structure or geysering events occur, which have implications for public safety and health as well as additional costs. Previous studies, including numerically and experimentally, on the mechanism of an air pocket entrapment includes Hamam and McCorquodale (1982), Cardle et al. (1989) and Li and McCorquodale (1999), among others. Overall, these studies indicated that hydraulic instability may occur due to transition from the free-surface flow to the pressurized flow in storm sewers. Moreover, it was found that the compression and expansion of trapped air bubbles in the sewer system produce high-frequency pressure transients.

The transition can be simulated using the Preissmann slot model (Cunge and Wegner, 1964). However, as shown by Vasconcelos et al. (2006), this model can result in spurious oscillations due to the narrow slot. The two-components pressure approach (TPA) is an alternative to overcome the inability of Preissman slot model in simulating the sub-atmospheric full pipe flow. In this shock capturing model, the hydrostatic pressure is decoupled from surcharged pressures in pressurized conditions (Vasconcelos and Wright, 2007). This approach is formed based on the fundamental similarity between unsteady incompressible flow equations for elastic pipe and the unsteady open-channel flow equations. The model predictions could capture the experimental data with a good agreement. However, this model is susceptible to oscillatory

behaviors, particularly, in the presence of high pressure wave speed (Bousso et al., 2013). The shock fitting approach was employed in numerous studies, e.g. Guo and Song (1990) and Fuamba (2002), in which two set of governing equations are used for free-surface and pressurized zones independently and the air-water interface is calculated iteratively by using an interpolation technique. However as indicated by Politano et al. (2007) and Bousso and Fuamba (2014), these interpolation does not conserve the mass continuity and generate significant errors. Using the mass and momentum conservation equations around the wavefront improves the accuracy (Bousso and Fuamba, 2014).

The main disadvantage of the above mentioned studies is that they result in a single phase model that do not explicitly account for the air effect on the hydraulic simulation. Instead the rigid column (RC) model let the air effect to be taken into account. This lumped-pressure model assumes a spatially invariant velocity, as those of Li and McCorquodale (1999) and Zhou et al. (2004). Vasconcelos and Leite (2012), experimentally and numerically, investigated the air pocket entrapment by a suddenly closed gate valve at the downstream. The RC model was applied, where the water and air volumes were assumed as two separate rigid columns at the upstream and downstream, respectively. Following the experiment of Vasconcelos and Leite (2012), Hatcher et al. (2015) numerically simulated the air pocket entrapment by suddenly closed a gate valve, using the RC model as well as the modified Saint-Venant equation set, solved by Method of Characteristic (MOC). Vasconcelos and Leite (2012) and Hatcher et al. (2015) predicted the solutions with reasonable tolerance of accuracy, except for the total valve closure, in which the numerical solutions did not exhibit damping and the peak pressures were overestimated significantly.

2 OBJECTIVES

As demonstrated by Karney (1990) and Malekpour and Karney (2014), after a specific length of a pressurized water column, the internal energy, stored in the water column, balances with the kinetic energy and the air pressure has to be equal to the maximum water hammer pressure. Thus, after this threshold length, the RC model overestimates the air pressure head and violates the physics of the flow, because it exceeds the maximum water hammer pressure. Meanwhile, the RC model is attractive since it is conceptually simple and easy to implement, while incorporates the fundamental features of the flow.

In this regard, a shocking fitting approach allows to compute the pressurized and free-surface flows separately, while they are linked by satisfying the momentum and mass conservations within the transient region. The primary goal of this investigation is to assess the accuracy of the shock fitting model in prediction of the flow features of a closed conduit transient flow following an air pocket entrapment. The calculated flow variables include the flowrate, pressure surge and the consecutive attenuations. The undertaken shock fitting approach combines the RC model applied to the upstream pressurized flow and the Saint-Venant equation set, solved by the MOC, applied to the downstream free-surface flow. It is expected to improve the numerical solutions, compared to the previous results obtained by the RC model, because the free-surface part is detached from the pressurized column which now has a shorter length. Therefore, the RC model is less likely to exceed the threshold length and the over-predicted peak pressure head would be improved. Furthermore, the free-surface flow allows to more accurately calculate the air pocket volume rate, which directly influences the air pressure variation.

A typical example for studying the air pocket entrapment is to obstruct the outflow using a gate valve. Therefore, the air pocket entrapment could be investigated for both partially and completely flow obstructions. The results of this investigation are compared to the experimental data as well as the RC model and modified Saint-Venant equations set, presented by Hatcher et al. (2015).

3 GENERAL DESCRIPTION

In the steady flow condition, the water, which is supplied by a constant flowrate (Q_i) from a reservoir with initial absolute pressure head (h_u) enters the pipeline in pressurized regime at the upstream. Somewhere along the pipeline at the downstream, the flow separates from the pipe wall and freely discharges to the atmosphere. Following the experiment of Hatcher et al. (2015), the pipeline diameters are set as $D = 53$ and 102 mm with the total length $L_t = 10.7$ m and $L_t = 12\ m$ and adverse slopes $S = -2$ and $S = -1.3$ %, respectively. The pipe material is clear PVC with Manning roughness coefficient $n = 0.009$. At the downstream end, a knife-gate valve with the same inside dimeter as the pipeline diameter is placed with initially no obstruction on the flow, while the valve is operated to certain closure degrees, i.e. 100 and 81%. The valve is assumed to operate in time linearly and to completely block the pipe cross-

section in 0.2 s (Vasconcelos and Leite, 2012). Note that the kinematic viscosity of water is set as $\vartheta = 10^{-6}\frac{m^2}{s}$.

3.1 INITIAL CONDITION

With respect to the initial conditions, the first challenge is to find the steady state solution for the free-surface flow. Alves et al. (1993) investigated the drift velocity of an air bubble in an inclined liquid column and they found the water surface profile for different inclination angles, including the horizontal one. Further detail is referred to Benjamin (1968) and Alves et al. (1993), and here it is only mentioned that the profile with zero inclination angle is taken as the steady state solution for all adverse slopes, because the undertaken slopes in this study is not so steep. Thus, so far, the initial water surface elevations, $y_i(x_i)$, at each x_i location are calculated. The initial air pocket volume is calculated using the following formula,

$$\forall_a^0 = A\left(L_t - L_{u,0}\right) - \int_{L_u}^{L_t} A_f(x)dx, \quad [1]$$

where, $\forall_a^0$ denotes the initial air volume and $L_{u,0}$ is the initial water column length. A represents the pipe cross section area and $A_f(x)$ represents the free-surface flow cross section area at the location x. Following the experiment (Hatcher et al., 2015) the initial air cavity volume is set to a certain amount, therefore, in Eq. [1] the initial pressurized water column length, $L_{u,0}$, is changed manually such that the value of the initial air volume is achieved.

The initial velocity, at each cross section can be calculated using the continuity equation as,

$$Q_i = V_i(x_i)A_f(x_i). \quad [2]$$

In terms of the pressurized column, the initial velocity, denoted by V_u, is calculated as,

$$Q_i = V_u A. \quad [3]$$

In order to calculate the initial absolute pressure head, $h_{u,0}$, the steady state momentum equation is applied to the pressurized water column as,

$$0 = \frac{h_{u,0} - h_{a,0}}{L_{u,0}} + \left[S - \left(\frac{f}{D} + \frac{K_{loss}}{L_{u,0}}\right)\frac{V_{u,0}|V_{u,0}|}{2g}\right], \quad [4]$$

where the subscript zero denotes the initial value, f and K_{loss} represent the Darcy friction factor and summation of local loss coefficients respectively and h_a represents the air pocket absolute pressure head, with initial value as the atmospheric pressure head, i.e. $h_{a,0} = 10$ m and g denotes the gravity acceleration constant, $g = 9.81\ \mathrm{ms}^{-2}$. The Darcy friction factor is calculated using the Colebrook-White formula as,

$$\frac{1}{\sqrt{f}} = -2\ log\left(\frac{2.51}{Re\sqrt{f}}\right), \quad [5]$$

where Re is the Reynolds number and it is calculated as $Re = \frac{V_u D}{\vartheta}$.

3.2 BOUNDARY CONDITIONS

At the upstream end, it is assumed that the flow is discharged into the reservoir constantly with flowrate (Q_i). At the downstream end, the valve is assumed to operate linearly, while it takes $0.2s$ to completely obstruct the outflow (Vasconcelos and Leite, 2012). The velocity at the downstream end at each time step, $V_{out}^{(n)}$, where superscript n denotes the time step interval, is calculated using the orifice discharge formula as,

$$V_{out}^{(n)} = c_d\sqrt{2g\left|h_a^{(n)} - h_{atm}\right|} \quad [6]$$

where c_d represents the discharge coefficient, $h_a^{(n)}$ is the air pocket absolute pressure head, calculated at the time step (n) and h_{atm} is the atmosphere pressure head $(h_{atm} = 10\,m)$. Following Zhang et al. (2018), the discharge coefficient is assumed as a function of the valve opening ratio, denoted by τ, with the maximum value $(\tau_{max} = 0.36)$ and the minimum value $(\tau_{min} = 0)$, corresponded to $\tau = 100$ and $\tau = 0$, respectively.

4 GOVERNING EQUATIONS

The undertaken approach in this study is a shock fitting approach, in which the pressurized column is simulated by an RC model and the free-surface flow is calculated using the Saint-Venant governing equations set, solved by MOC method. The Saint-Venant governing equations set which is applied to the downstream free-surface flow has a form as (Chaudhry, 2008),

$$\frac{\partial y}{\partial t} + V\frac{\partial y}{\partial x} + D_h\frac{\partial V}{\partial x} = 0, \quad [7]$$

$$\frac{\partial V}{\partial t} + V\frac{\partial V}{\partial x} + g\frac{\partial y}{\partial x} = g(S - S_f),$$

where y and V represent the flow depth and velocity, respectively, varying along the flow direction x. D_h is the hydraulic depth, calculated as $D_h = {}^{A}/_{B}$, where B denotes the water surface width and S_f is the friction slope, calculated at each cross section using the Chézy formula as,

$$S_f = n^2\frac{V^2}{R_h^{4/3}}, \quad [8]$$

where R_h is the hydraulic radius.

The main concept of the RC model is to neglect the water compressibility so that the pressurized flow could be treated as a rigid column with space-invariant velocity. Applying the momentum conservation law to this rigid column yields an equation as,

$$\frac{dV_u}{dt} = \mathrm{g}\frac{h_u - h_a}{L_u} + \mathrm{g}\left[S - \left(\frac{f}{D} + \frac{K_{loss}}{L_u}\right)\frac{V_u|V_u|}{2g}\right], \quad [9]$$

where t represents the time variable. The pressure head of the upstream column (h_u) is calculated using the inflow hydrograph of the upstream reservoir. Thus,

$$A_s\frac{dh_u}{dt} = Q_i - AV_u, \quad [10]$$

where A_s represents the cross section area of the reservoir, here assumed as $A_s = 60A$. Following Vasconcelos and Leite (2012) and Hatcher et al. (2015), the air pocket is assumed to undergo the compression in a Polytropic process. Thus,

$$h_a\forall_a^k = cte, \quad [11]$$

where k represents the Polytropic coefficient, which is set as $k = 1.2$ (Vasconcelos and Leite, 2012).

As mentioned before, in the shock fitting approach, the upstream pressurized column and the downstream free-surface flow are connected by a transient region, where the celerity of the wave front as

well as the water depth and velocity for the first node of the free-surface flow will be calculated using three extra equations. First, the mass conservation law gives the celerity of the wave front as,

$$W = \frac{AV_u - A_1V_1}{A - A_1}, \qquad [12]$$

in which W represents the celerity and the subscript $_1$ denotes the first node of the free-surface flow.

Li and McCorquodale (1999) elaborately developed the RC model for different transient stages, particularly, for the transition of a free-surface flow to a pressurized flow, in which they applied the momentum conservation law on the moving air-water interface. Moreover, Li and McCorquodale (1999) took the air pocket velocity into account. Thus, following Li and McCorquodale (1999), in the present paper a similar equation is used to find the water depth at the first node (y_1) as follows,

$$A(V_u - W - V_b)(V_1 - V_u) = gA(h_u - h_a) - A_1\frac{gy_1}{2} + g\Delta x\left(S - S_{f,1}\right)\frac{(A + A_1)}{2}, \qquad [13]$$

where V_b represents the air pocket velocity and Δx is the grid size. One may notice that one more equation is needed to calculate the velocity at the first node (V_1) of the free-surface flow. This equation, given by the positive characteristic of MOC method applied to the free-surface flow, will be explained in the next section.

Finally, the continuity equation applied to the pressurized column gives the time dependent equation for the rigid column length as,

$$A\frac{dL_u}{dt} = W + V_b. \qquad [14]$$

5 NUMERICAL SIMULATIONS

As mentioned before, the Saint-Venant equations set of the free-surface flow is solved using the MOC method. To find the dependent variables in time-space coordinates, this method transforms the governing equations [7] into two ordinary differential equations (ODEs), called compatibility equations, that can be integrated along the characteristic curves. Further details of this method could be found in the reference book (Chaudhry, 2008). The compatible equations of [7] are as,

$$\frac{DV}{Dt} + \frac{g}{c}\frac{Dy}{Dt} = g\left(S - S_f\right), \qquad [15]$$

$$\frac{DV}{Dt} - \frac{g}{c}\frac{Dy}{Dt} = g\left(S - S_f\right),$$

where c denotes the gravity wave celerity $c = \sqrt{g\frac{A}{B}}$. Note that the derivatives of the independent variables (x, t) have been changed to a new derivative along the characteristic paths, thus, $\frac{D}{Dt} = \frac{\partial}{\partial t} + \frac{\partial}{\partial x}\frac{dx}{dt}$, in which, the positive and negative characteristic paths could be found as follows, respectively.

$$\frac{dx}{dt} = V + c, \qquad [16]$$

$$\frac{dx}{dt} = V - c.$$

In any position where the two characteristic lines intersect each other, the dependent variables, V and y, can be calculated simultaneously. The finite difference solution of the compatibility equations can be found using a finite difference computational mesh depicted in Figure 1.

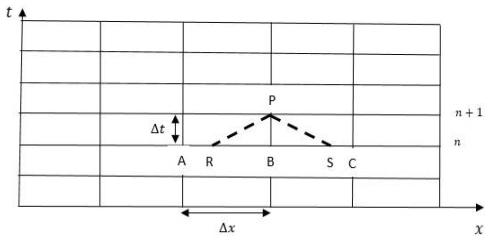

Figure 1: Characteristic lines in a computational mesh

As illustrated in Figure 1, the unknown variables at the time step $n+1$ for a grid point (P) can be calculated using the solutions at R and S which are associated with the time step n. As can be seen, the characteristic lines do not intersect the time lines at the grid points A and B. Therefore, the solutions at R and S need to be interpolated using the solutions at the grid points. Note that in this paper the linear interpolation technique has been utilized. The discrete equations can then be written as follows (Chaudhry, 2008),

$$V_p = D_q - D_A y_P, \quad [17]$$

$$V_p = D_n + D_B y_P, \quad [18]$$

where

$$D_q = V_R + \frac{g}{c_R} y_R + g(S - S_f)_R \Delta t \quad \text{and} \quad D_A = \frac{g}{c_A}, \quad [19]$$

$$D_n = V_S - \frac{g}{c_S} y_S + g\left(S - S_f\right)_S \Delta t \quad \text{and} \quad D_B = \frac{g}{c_B}, \quad [20]$$

where

$$\varphi_R = \varphi_B + (V + c)\frac{\Delta t}{\Delta x}(\varphi_A - \varphi_B), \quad [21]$$

$$\varphi_S = \varphi_B + (V - c)\frac{\Delta t}{\Delta x}(\varphi_C - \varphi_B), \quad [22]$$

where φ could be either V or y. Note that Δt represents the time step increment which is calculated using the courant-friedrichs-lewy (CFL) condition. This condition for the free-surface flow is as,

$$CFL = [\max(V) + \max(c)]\frac{\Delta t}{\Delta x}, \quad [23]$$

where $\max$ denotes the maximum value. As explained in the Section 4, at each time step, the water depth at the first grid point (y_1) is calculated using the momentum balance in the transient region, Eq. [13]. Meanwhile, Figure 1 illustrates that only the negative characteristic path transfers the solutions to the first grid point. Therefore, Eqs. [18], [20] and [22] yield an equation to find the velocity at the first grid point and at the time step $n+1$.

Similarly, in the last grid point, only the positive characteristic path transfers the solution to the last grid point, in which the velocity is calculated using the orifice-like equation [6]. Thus, using Eq. [17], [19] and [21] yields an equation to calculate the water depth at the time step $n+1$ and at the last grid point i_{max}, $(y_{i_{max}})$, where i_{max} represents the number of the last grid point located at the outlet.

The governing equations of the pressurized column, Eqs. [9], [10] and [14], are solved using the backward Euler (BE) scheme. Considering a general ODE problem as,

$$\frac{d\varphi}{dt} = f(\varphi). \quad [24]$$

The BE scheme applied to [24] yields the discrete formula as,

$$\varphi^{n+1} = \varphi^n + \Delta t f(\varphi^{n+1}), \quad [25]$$

where the superscript indicates the level of the time step. After calculating the water depth profile, the volume of the air pocket at the time step $n+1$ is calculated using the following formula,

$$\forall_a^{n+1} = A(L_t - L_u^{n+1}) - \int_{x_1}^{x_{i_{max}}} A^{n+1}(x)dx - (W^{n+1} + V_b^{n+1})\Delta t(A - A_1^{n+1}). \quad [26]$$

Then, the air pocket pressure head at the time step $n+1$ is calculated as,

$$h_a^{n+1}(\forall_a^{n+1})^k = h_a^n(\forall_a^n)^k \quad [27]$$

It is worth mentioning that due to the implicit time integration scheme, an iterative approach is needed, in which all discrete equations will be solved simultaneously up to a certain tolerance ($Tol = 10^{-15}$). The tolerance ensures that the numerical errors are suppressed and the solutions are accurate enough.

6 RESULTS AND DISCUSSIONS

The proposed shock fitting approach, hereafter called RC-FM, was tested with partial valve closure (81%) and total valve closure (100%). The results of this approach are compared to the experimental and numerical results provided by Hatcher et al. (2015). Hatcher et al. (2015) applied a rigid column model, hereafter called RC, to the entire closed conduit flow, assuming the water and air pocket as two separate columns. In the other model, studied by Hatcher et al. (2015), hereafter called MOC, the modified Saint Venant equations, was solved by the MOC method throughout the pipeline in order to incorporate the effects of the pipe elasticity and water compressibility, through considering the water hammer speed (a) instead of the gravity wave celerity. The performance of RC-FM is assessed by comparing the peak pressure head (maximum and minimum) and flowrate for two different pipeline diameters ($D = 53 \,\&\, 102\ mm$), each with two different initial air pocket volumes and two different initial flowrates. The distributions of the normalized air pressure head $\left(\frac{H_a}{D}\right)$ and the normalized discharge flowrate $\left(Q^* = \frac{Q}{\sqrt{gD^5}}\right)$ are presented in terms of the normalized time variable $\left(T^* = \frac{\sqrt{gD}}{\sqrt[3]{\forall_{a,0}}}t\right)$.

For the total valve closure, the air pressure head distributions, provided by the above mentioned approaches, are illustrated in Figure 2. According to Vasconcelos and Leite (2012), the valve takes $0.2s$ to completely block the outlet. Thus, as can be seen in Figure 2, the pressure head and flowrate, calculated by RC-FM do not vary for a small time interval along the horizontal axis. This fact indicates that in the computation, the selected time step is smaller than $0.2s$ and the valve takes some time to touch the flow, during which the air pocket has contact with the atmosphere and the air pressure is the same as the atmosphere.

In both cases with different air pocket volumes and flowrates, the MOC and RC models over predict the maximum and minimum pressures, while the RC-FM could improve these peak pressures relatively. Moreover, the RC-FM approach could predict the attenuated solutions, which makes the results in the next oscillations more accurate, while the RC and MOC do not exhibit any damping effect. Note that the damping effect of the RC-FM is larger than the experiment.

For the larger air pocket sizes, the pressure frequencies are predicted more accurately by all approaches. However, for the smaller air pocket sizes, the RC model fails to predict the frequency properly, while the MOC model prediction of the pressure frequencies is accurate, which could be due to incorporating the water hammer speed. Surprisingly, the RC-FM approach, which only include the gravity wave celerity, could predict the pressure frequencies as well even for the small air pocket sizes. This could be due to taking the air velocity into account through the variable V_b, which compensates for neglecting the pipe elasticity and water compressibility.

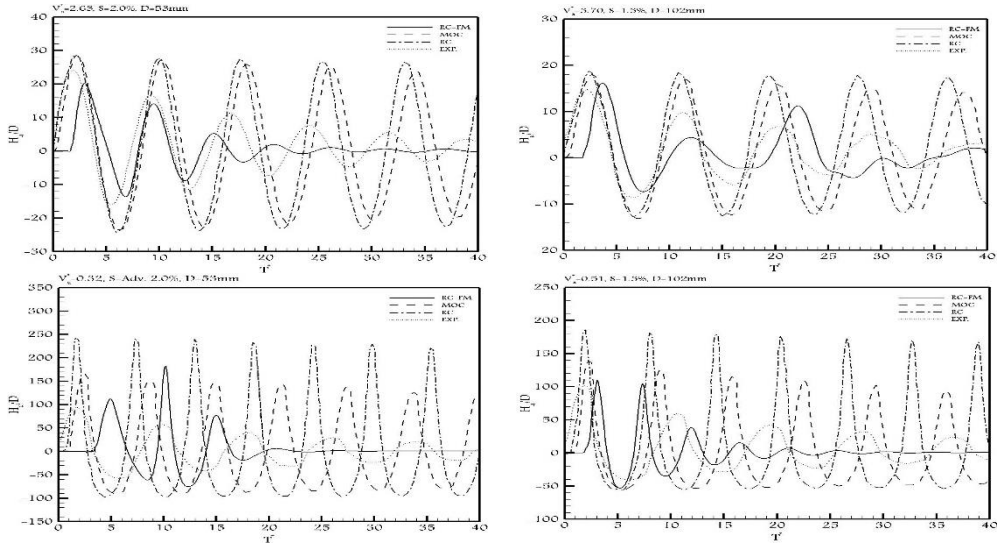

Figure 2: Pressure hydrograph for total valve closure.

The distributions of the discharge flowrate are presented in Figure 3 for all numerical models and the experiment. The initial experimental flowrates were used as an input of the numerical models. For the minimum and maximum flow rates, the RC-FM approach outperforms the MOC and RC models for both air pocket sizes, while the MOC is more accurate compared to the RC model, particularly, in smaller air pocket sizes, since the RC model significantly over predicts peak flow rates. It is clear that the RC-FM captures the decay of inertial frequencies more accurately than the MOC and RC models, although it is more rapidly than the experiment. The discrepancies in frequencies of discharge flowrate is similar to the pressure head.

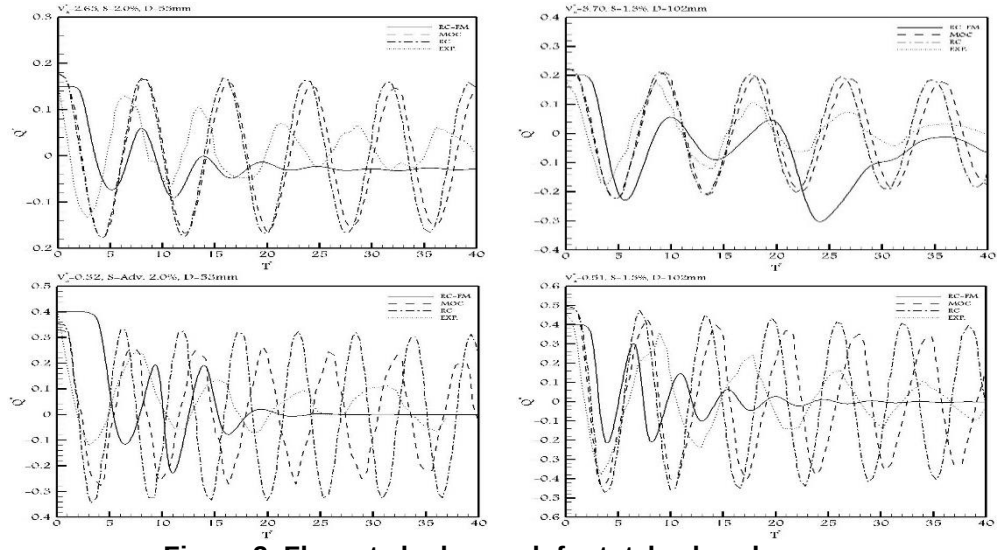

Figure 3: Flowrate hydrograph for total valve closure.

The RC-FM approach was also examined in computation of partially valve closure 81%. The results were compared to the MOC and RC models as well. Figure 4 illustrates the distribution of the pressure head. The MOC and RC are more accurate than the RC-FM approach in larger air volume, although all models under predict the peak pressure head. For smaller air volume, the RC-FM approach significantly under predicts the peak pressure head, while the MOC and RC over predict the peak pressure head. For the partial valve closure, attenuation is mostly caused by the kinetic energy release from the outlet, which is well accounted for in all models. However, the RC-FM approach predicted the transition to steady state conditions after valve closure more accurately, except for two cases, in which the RC-FM is still competitive to the RC and MOC models.

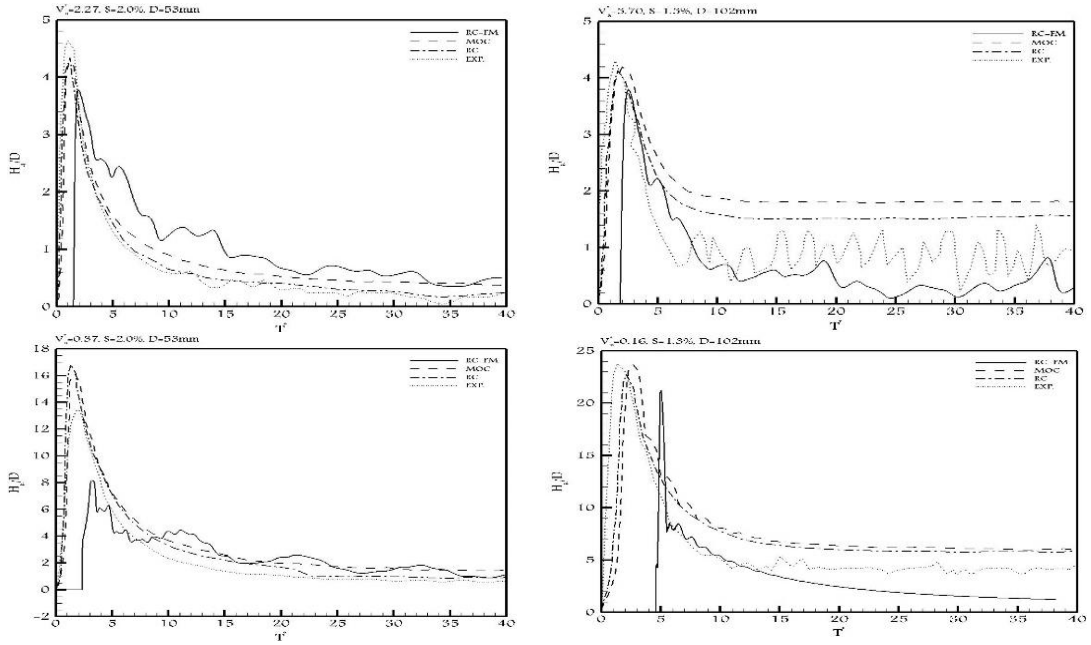

Figure 4: Pressure hydrograph for 81% valve closure.

The discharge flowrate distribution for 81% closure is illustrated in Figure 5. As can be seen the MOC and RC models behaves more accurately than the RC-FM approach. Steady state flow rates were also more accurately predicted by MOC and RC.

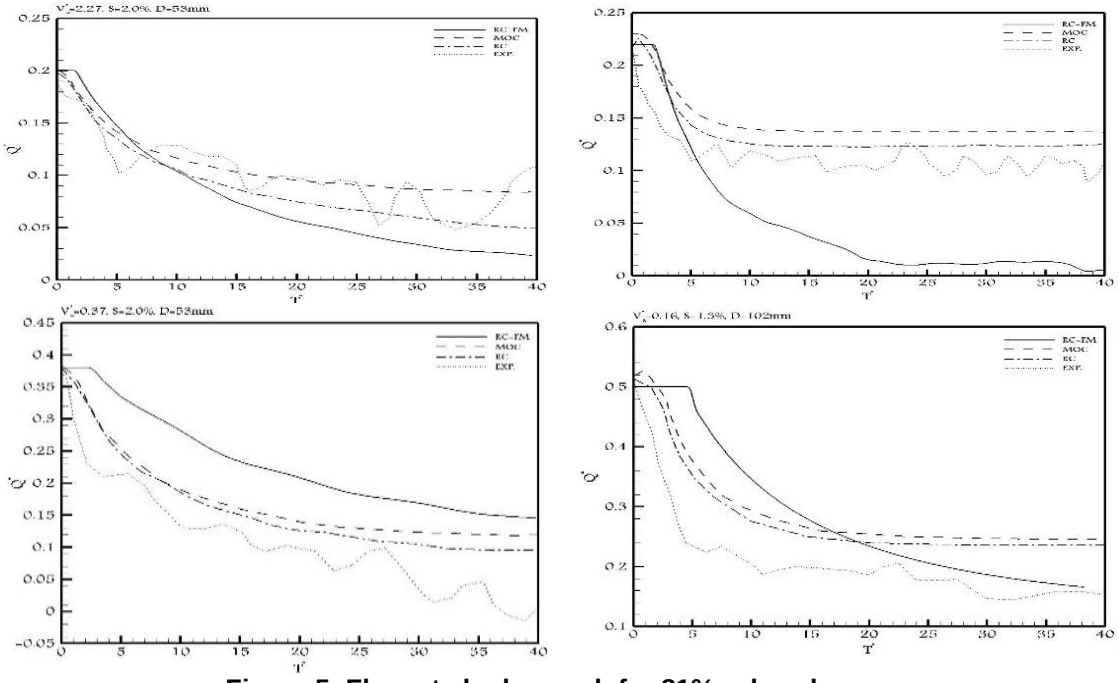

Figure 5: Flowrate hydrograph for 81% valve closure.

7 CONCLUSIONS

Surges caused by sudden air pocket compression were studied for $D = 53$ and $102\ mm$ PVC pipelines with adverse slopes. A shock fitting approach (RC-FM) was proposed in which the rigid column model and the Saint-Venant equations were applied to the pressurized flow and the free surface flow, respectively. The results were compared to the experiments and numerical results of rigid column (RC) model and modified Saint-Venant equations (MOC) of Hatcher et al. (2015). A constant inflow discharge was supplied by an upstream reservoir in which a pressurized flow existed at the upstream end of 10.7 or $12.0\ m$ pipelines and a free surface flow at the downstream end. Sudden closures of a downstream valve initiated the surge event trapping an air pocket. Two different air pocket volumes and flow rates were tested for 81% and 100% valve closures. The objective was to determine the abilities of the shock fitting approach focusing on peak surge pressures, flowrates. For total valve closures, the shock fitting approach predicts the peak pressure head and flowrates more accurately for various ranges of air volumes and discharge flowrates, while both RC and MOC models consistently overestimated. Moreover, the accuracy of MOC and RC models decreased for cases with larger flowrates and smaller air pocket volumes. Inertial frequencies were resolved accurately by all models for cases with smaller flowrates and larger air pocket volumes. However, for small air pocket sizes, the RC model significantly diverged, since the predicted frequencies are larger than the experiments. The RC-FM approach could capture the attenuation behavior, although this approach dampens the solutions more rapidly than the experiment. Both MOC and RC models was unable to predict this attenuation. Both MOC and RC models performed more accurately for partial valve closure cases.

In conclusion, for the total valve closure the proposed shock fitting approach captures the flow features of air entrapment more accurately for various ranges of air pocket volumes and discharge flowrates, due to its ability to take the air velocity into account. However, it does not work well for partially closed valve, as it under estimates the peak pressure, although, it could predict the steady state condition competitively. This poor behavior could be due to the discharge coefficient, since the computation is sensitive to this coefficient.

ACKNOLEDGEMENTS

The writers would like to express their gratitude to the Natural Sciences and Engineering Research Council of Canada (NSERC) for the financial support.

REFERENCES

Bousso, S., Daynou, M. and Fuamba, M., (2013). Numerical Modeling of Mixed Flows in Storm Water Systems: Critical Review of Literature*, J. Hyd. Eng.,* 139(4), 385-396.

Bousso, S. and Fuamba, M., (2014). Numerical and Experimental Analysis of the Pressurized Wave Front in a Circular Pipe, *J. Hyd. Eng.*, 140(3), 300-312.

Cardle, J. A., Song, C. C. S., and Yuan, M. (1989). Measurements of mixed transient flows, *J. Hyd. Eng.*, 115(2), 169–182.

Cunge, J. A., and Wegner, M. (1964). Numerical integration of Barre de Saint-Venant's flow equations by means of implicit scheme of finite differences. *Houille Blanche*, 19(1), 33–39.

Fuamba, M. (2002). Contribution on transient flow modelling in storm sewers, *J. Hyd. Res.,* 40(6), 685–693.

Guo, Q., and Song, C. C. S. (1990). Surging in urban storm drainage systems, *J. Hyd. Eng.,* 116(12), 1523–1539.

Hamam M.A. and McCorquodale J. A. (1982). Transient conditions in the transition from gravity to surcharged sewer flow*, Canadian Journal of Civil Engineering*, 9, 189-196.

Hatcher, T. M., Malekpour, A., Vasconcelos, J. G. and Karney, B. W. (2015). Comparing Unsteady Modeling Approaches of Surges Caused by Sudden Air Pocket Compression, *J. Water Management Modeling C392*. doi: 10.14796/JWMM.C392.

Karney, B. W., (1990). Energy Relations in Transient Closed-Conduit Flow, *J. Hyd. Eng.*, 116(10), 1180-1196.

Li, J., and McCorquodale, A. (1999). Modeling mixed flow in storm sewers, *J. Hyd. Eng.*, 125(11), 1170–1180.

Malekpour, A. and Karney, B. W., (2014). Discussion of 'Pressure Surges Following Sudden Air Pocket Entrapment in Storm-Water Tunnels' by José G. Vasconcelos and Gabriel M. Leite, *Journal of Hyd. Eng.,* 140 (4), 1081–9.

Politano, M., Odgaard, A. J., and Klecan, W. (2007). Case study: Numerical evaluation of hydraulic transients in a combined sewer overflow tunnel system, *J. Hyd. Eng.*, 133(10), 1103–1110.
Vasconcelos, J. G., Wright, S. J., and Roe, P. L. (2006). Current issues on modeling extreme inflows in stormwater systems. *Intelligent modeling of urban water systems*, monograph 14, W. James, K. N. Irvine, E. A. Mc Bean, and R. E. Pitt, eds., Guelph, ON, Canada.
Vasconcelos, J. G. and Wright, S. J. (2007). Comparison between the two-component pressure approach and current transient flow solvers, *J. Hydraulic Research*, 45(2), 178–187.
Zhou, F., Hicks, F., and Steffler, P. (2004). Analysis of effects of air pocket on hydraulic failure of urban drainage infrastructure, *Can. J. Civ. Eng.*, 31(1), 86–94.
Vasconcelos, J. G., and Leite, G. M., (2012). Pressure Surges Following Sudden Air Pocket Entrapment in Storm-Water Tunnels, *J. Hyd. Eng.*, 138(12), 1081-1089.